

XMM Optical Monitor

MULLARD SPACE SCIENCE LABORATORY
UNIVERSITY COLLEGE LONDON

Author: H.Kawakami & J.Fordham

Flat Field coincidence loss in the MIC detector for XMM-OM

DOCUMENT: XMM-OM/MSSL/TC/0050.01 17-Nov-98

XMM Optical Monitor

MULLARD SPACE SCIENCE LABORATORY
UNIVERSITY COLLEGE LONDON

Author: H.Kawakami & J.Fordham

Flat Field coincidence loss in the MIC detector for XMM-OM

DOCUMENT: XMM-OM/MSSL/TC/0050.01 17-Nov-98

<< Flat field coincidence loss in the MIC detector for XMM-OM >>

Hajime KAWAKAMI and John Fordham

1. Introduction

Spatial coincidence between events in the MIC photon counting detector can be placed in two categories, namely

A) Unresolved coincidence; the footprints of the separate events merge together and the event peaks can be no longer separated when sampled by the CCD pixels. If two events fall into neighbouring CCD pixels then they are always merged together.

B) Resolved coincidence; the footprints of the separate events overlap only in the wings and, in the CCD data, the events peaks are distinguishable. Both events are counted without loss but their centroided positions are displaced because of the contamination.

The level of coincidence is dependent not only on the distance between events but also on :

- * the pulse energies of the events involved,
- * on their relative positions within the CCD array,
- * on the number of events involved; two, three or more
- * the event profile for a particular intensifier.

Although a number of artefacts affect the probability of coincidence, it is useful to introduce the parameter "effective coincidence area" (see [1] Moorhead et. al. 1998) that allow the relationship between input and detected events for diffused objects (or flat fields) to be governed by a simple equation. This also enables simple modelling of the coincidence between adjacent stars.

2. Experiments and analysis

A number of F-F images at different count rates were acquired in photon counting mode using the EOB-1 MIC system, which incorporates a Thomson CCD. The energy in a 3x3 pixel array, centred on each event, is used for event detection. The input light source was a Deuterium lamp installed in the monochrometer. The wavelength was 5800Å. The intensity was tuned by changing the width of the entrance slit. The intensity of the input light was monitored by a reference photo-diode. A 10x10mm square region within each acquired image was used for data analysis. The alignment of the mask pattern to the detector was not ideal (see Figure 1). Therefore the CCD camera format in the vertical direction had to be larger than the 129 vertical rows corresponding to 10mm. The pulse height distributions for both intensifiers are shown in Figures 2a and 2b. The pulse height distribution for the DEP_#7 intensifier was broader than that of the DEP_#6 intensifier, which means less saturation of the intensifier. This might have resulted in a smaller event size, hence

lower coincidence.

From the relationship between input light level and detected count rate, the probability for unresolved coincidence leading to loss of data was determined, and the effective coincidence area derived with the help of equation (A-2).

Table 1 gives the data on DEP_#6 intensifier. This data was acquired with a CCD camera format of 256(H)x150(V). Table 2 is for DEP_#7 intensifier, a CCD camera format of 256(H)x156(V) being employed for data acquisition. Columns 2 and 3 show the direct data. The 4th column is the detection probability assuming, at the lowest count rate, that no data is lost (i.e. probability = 1). The 5th column introduces a small correction to allow for coincidence at the lowest count rate, namely 0.9795861 instead of 1.00 in Table 1.

The final (6th) column is the best theoretical fit to the acquired data using Equation (A-2) in Appendix 1, resulting in a scale frequency, 'a' (see below), of 220kHz for the DEP_#6 intensifier and 272kHz for the DEP_#7 intensifier, that then defines the area for unresolved coincidence. Figs. 3 and 4 show the affect of coincidence on a F-F at a high input data rate for the 2 DEP intensifiers.

From Appendix 2, the CCD camera frame period is calculated to be 6.6114ms (=151.25389Hz) for the DEP_#6 tube and 6.8526ms(=145.9300Hz) for the #7 tube.

From Equation (A-2), the scale frequency is described as

$$a = \frac{S F}{s}$$

where,

F: CCD frame rate

s= area for unresolved coincidence = effective coincidence area

S: area of F-F image

In the case of the DEP_#6 tube,

$$s = \frac{S F}{a} = \frac{(10 \times 10 \text{mm}^2) (151.25389 \text{Hz})}{220 \text{ kHz}} = 68751.8 \text{ um}^2$$

$$\text{Area of a CCD pixel} = (23 \text{um} \times \overset{3.37}{\cancel{3.08}})^2 = \overset{6007.8001}{5018.3056} \text{ um}^2$$

Therefore, $s = 13.70 \text{ (CCD pixel)}^2$.

Effective coincidence radius = 2.088 (CCD pixel)

In the case of the DEP_#7 tube,

$$s = \frac{(10 \times 10 \text{mm}^2) (145.9300 \text{Hz})}{272 \text{ kHz}} = 53650.7 \text{ um}^2 = 10.69 \text{ (CCD pixel)}^2$$

Effective coincidence radius = 1.845 (CCD pixel)

3. Discussion

3.1 Dynamic range

Applying the F-F mathematical model to the experimental data results in a sensible value for the effective coincidence area when event energy is used for event detection. This shows the validity of the model, the excellent fit being enhanced by the physical characteristics of the image intensifier, i.e. very fast phosphor screen and negligible pore paralysis in the MCPs at the illumination levels used. The non-linearity of the dynamic range curve at all input flux rates due to coincidence loss even at low rates (i.e. 2 - 5% at 10-20kHz) is, however, clearly shown.

For XMM-OM, the MIC detector will suffer appreciable loss, particularly at high input intensity, the level being dependent upon filter selection and object brightness. Therefore, it is essential to convert the detected flux to real flux for precision photometry. One of the problems associated is the stability of the "scale frequency". The authors believe the smaller event size on the DEP_#7 tube is mainly due to less saturation in the MCPs. The voltages applied to the FM intensifiers will need to be increased during the lifetime of the observatory to compensate for gain depletion in the MCPs leading to more saturation in the MCPs and probable increase in event size. To allow for this the F-F linearity curve may need updating at intervals using well characterized diffuse astronomical objects.

It should be noted that the highest count rate used in the experiments was 126722.50 cnts/sec/cm² with the DEP_#6 intensifier. Here, equation (A-1) shows that 74% of coincidences are double. At higher count rates, the probability of triple and quadruple coincidence increases and associated is a larger effective coincidence area as the 3rd/4th events can create bridges between the previous 2nd/3rd resolved events. Therefore, the coincidence area given in this report is adequate for modelling of double coincidence but may have errors when triple or quad coincidences become appreciable.

For point sources, the mathematical model is simpler than that for F-F or extended sources. It does not depend on an effective coincidence area or intensifier characteristics and accommodates the affect of double or triple coincidences. However, observing high count rate point sources will stress the image intensifier and pore paralysis in the MCPs, which is not accommodated in the model, will become a factor.

For ground based astronomical applications, the input flux rate from a source is a variable, fluctuating primarily due to the seeing. This makes precise photometry using the dynamic range curve difficult. However, for XMM-OM, the star images and flux will remain constant. Hence, if the simple model is confirmed with the FM intensifiers, it will be valid for use with both FM intensifiers over the 10 year period.

At present, the model for F-F illumination has only been confirmed using experimental data. It is expected that the dynamic range curve for point sources will be used much more often during data analysis. Therefore it is essential that experimental data on a point source input must be obtained as soon as possible to validate that model.

3.2 Application to event width measurement

It is almost impossible to determine the event width on the intensifier output directly if the event profile is under-sampled by the CCD as is the case for the MIC system where the event width is tuned to be 1.0-1.2 CCD pixels. We have previously proposed a method to determine the average event width from the fine structure of the centroiding LUT curves that describe the relationship between real and calculated event positions (see Kawakami et. al.1994, Michel et. al. 1997).

The F-F coincidence approach described in this report can be used as a second method for determining event width when under-sampled. As has been shown, using this approach the difference in event width between the DEP_#6 and DEP_#7 intensifiers is clearly detected.

References.

- [1] Moorhead C., Fordham J., Galbraith R., 1998, to be submitted.
- [2] Kawakami H., Bone D., Fordham J., Michel R., 1994, Nuclear Instr. and Meth. A, 348, p707.
- [3] Michel R., Fordham H., Kawakami H., 1997, Mon. Not. R. Astron. Soc., 292, p611.

Table 1.

DEP_#6 tube CCD 256(H)x150(V) 17:03-17:33 30 Sep. 1998
 Th=18ADU 3x3 Energy centroiding

	MIC Detected count rate (cnts/sec)	Ph-diode current (fA)	Detection probability relative to lowest rate	Detection probability	Fitting with a=220kHz
1	126722.50	383.20	.6858220	.6718217	.6714945
2	95072.00	254.80	.7739049	.7581064	.7622249
3	79892.10	202.50	.8181818	.8014795	.8041192
4	61496.60	145.60	.8759303	.8580492	.8534496
5	42105.00	95.60	.9134244	.8947778	.9002878
6	33377.10	72.00	.9635422	.9438725	.9237705
7	19909.35	41.70	.9901084	.9698964	.9547648
8	8920.60	18.50	1.0000000	.9795861	.9795861

Table 2.

DEP_#7 tube CCD 256(H)x156(V) 14:34-15:16 20 Oct. 1998
 Th=18ADU 3x3 Energy centroiding

	MIC Detected count rate (cnts/sec)	Ph-diode current (fA)	Detection probability relative to lowest rate	Detection probability	Fitting with a=272kHz
1	91142.55	254.75	.8326462	.8184370	.8205877
2	77139.75	207.55	.8649963	.8502350	.8503162
3	67516.25	177.25	.8862458	.8711220	.8701484
4	59707.75	154.60	.8988267	.8834881	.8854490
5	49654.20	126.40	.9145787	.8989714	.9050036
6	43139.95	109.25	.9185960	.9029201	.9170967
7	34028.05	82.75	.9566550	.9403297	.9363336
8	22261.35	52.95	.9789619	.9622558	.9586537
9	9230.30	21.50	1.0000000	.9829350	.9829350

Appendix 1. Coincidence probability for F-F

Here we focus on a particular event within a CCD frame and consider whether it is suffering from unresolved coincidence or not.

Assume a coincidence area "s", within which other events in the same CCD frame cause an unresolved coincidence with that particular event. Assume also that "n" events fell within the area "s" in "N" CCD frames.

Excluding the event being focussed on, the probability of the remaining "n-1" events falling in the remaining "N-1" frames is

$$1. \text{ single event} \quad P1 = \left(\frac{N-1}{N} \right)^{(n-1)} = \left(1 - \frac{1}{N} \right)^{(n-1)}$$

The probability of only one of the remaining "n-1" events falling in the same CCD frame is

$$2. \text{ double coincidence} \quad P2 = C(n-1,1) * (1/N) * \{(N-1)/N\}^{(n-2)}$$

The probability of only two of the remaining "n-1" events falling in the same CCD frame is

$$3. \text{ triple coincidence} \quad P3 = C(n-1,2) * (1/N)^2 * \{(N-1)/N\}^{(n-3)}$$

The probability of only three of the remaining "n-1" events falling in the same CCD frame is

$$4. \text{ quadruple coincidence} \quad P4 = C(n-1,3) * (1/N)^3 * \{(N-1)/N\}^{(n-4)}$$

Now, introducing a parameter $p=n/N$, the above equations can be written as

$$P1 = \left(1 - \frac{1}{N} \right)^{(pN-1)} \implies \exp(-p), \quad \text{when } N \text{ and } n \text{ ----> infinity}$$

$$P2 = \frac{n-1}{1! N} \left(1 - \frac{1}{N} \right)^{(pN-2)} \implies p \exp(-p)$$

$$P3 = \frac{(n-1)(n-2)}{2! N^2} \left(1 - \frac{1}{N} \right)^{(pN-3)} \implies \frac{p^2}{2!} \exp(-p)$$

$$P4 = \frac{(n-1)(n-2)(n-3)}{3! N^3} \left(1 - \frac{1}{N} \right)^{(pN-4)} \implies \frac{p^3}{3!} \exp(-p)$$

$$P5 = \frac{(n-1)(n-2)(n-3)(n-4)}{4! N^4} \left(1 - \frac{1}{N}\right)^{(pN-5)} \implies \frac{p^4}{4!} \exp(-p)$$

$$P6 = \frac{(n-1)(n-2)(n-3)(n-4)(n-5)}{5! N^5} \left(1 - \frac{1}{N}\right)^{(pN-5)} \implies \frac{p^5}{5!} \exp(-p)$$

Now, with the MIC detector, one event out of two is still detected in the case of double coincidence, one out of three for triple coincidence, one out of four for quadruple coincidence, and so on. Therefore the detection probability can be written as,

$$\frac{n_{det}}{n} = \left[1 + \frac{p}{2!} + \frac{p^2}{3!} + \frac{p^3}{4!} + \frac{p^4}{5!} + \frac{p^5}{6!} + \dots \right] \exp(-p) \quad (\text{Eq. A-1})$$

$$= \frac{\exp(p) - 1}{p} \exp(-p) = \frac{1 - \exp(-p)}{p}$$

where, n_{det} denotes detected events.

For the convenience of application to experiment data, we assume "S" as the area of the F-F image, "x" as the event flux within the area S, "F" as the CCD frame rate and "t" as the integration time. Then,

$$p = n/N = \left(\frac{t s x}{S}\right) / (t F) = \frac{s}{S F} x = x/a$$

Finally the detection probability is described as,

$$\frac{n_{det}}{n} = \frac{x_{det}}{x} = \frac{1 - \exp(-x/a)}{x/a} \quad (\text{Eq. A-2})$$

where, $a = \frac{S F}{s}$

and x_{det} denotes detected flux from the area "S".

Summary of definitions :

- x = input data (photons/sec) within the area "S".
- F = CCD frame rate
- s = area for unresolved coincidence
- S = area of F-F image
- a = scale frequency

If $S/s = 1$, the equation then gives the detection probability for a point source. Namely,

$$\frac{n_{\text{det}}}{n} = \frac{x_{\text{det}}}{x} = \frac{1 - \exp(-x/F)}{x/F} \quad (\text{Eq. A-3})$$

where x_{det} denotes detected flux from the point source.

The equation can be modified as follows, which is suitable for the estimation of real input flux from a star,

$$\frac{x}{F} = -\ln\left(1 - \frac{x_{\text{det}}}{F}\right) \quad (\text{Eq. A-4})$$

It should be noted that, as x_{det} is always smaller than the frame rate "F", the value for the logarithm does not become negative.

Appendix 2. CCD frame rate

<< Thomson CCD camera EOB-1 Camera (Single Window) >>

1 vertical clock	800ns		
1 horizontal clock	100ns		
total vertical clocks for		FT period	288V
flash one row after FT			402H
flash two rows before the window			2x402H
total S-vertical clocks during readout period			288V
total horizontal clocks for one row			402H

Note) FT:Frame Transfer

frame time = FT + one flash after FT + two flash before window
+ S-vertical clocks during readout + H-clocks for readout

Examples)

a) If reading out full CCD area,
frame time = $800\text{ns} \times 288\text{V} + (1+2) \times 100\text{ns} \times 402\text{H}$
+ $800\text{ns} \times 288\text{V} + (100\text{ns} \times 402\text{H}) \times 288\text{V}$
= 12.1590ms

b) If reading out a 32 row CCD area
frame time = $800\text{ns} \times 288\text{V} + (1+2) \times 100\text{ns} \times 402\text{H}$
+ $800\text{ns} \times 288\text{V} + (100\text{ns} \times 402\text{H}) \times 32\text{V}$
= 1.8678ms

c) If reading out a 156 row CCD area
frame time = $800\text{ns} \times 288\text{V} + (1+2) \times 100\text{ns} \times 402\text{H}$
+ $800\text{ns} \times 288\text{V} + (100\text{ns} \times 402\text{H}) \times 156\text{V}$
= 6.8526ms

When considering a point source, the frame transfer period becomes a dead time when using a fast (e.g. P46) phosphor screen on the intensifier output. The dead time ratio is

$$\begin{aligned} (\text{FT time}) / (\text{frame time}) &= 0.2304\text{ms}/12.1590\text{ms} \\ &= 0.01895 && \text{for full area readout} \\ &= 0.2304\text{ms}/6.8526\text{ms} \\ &= 0.03362 && \text{for 156V area readout} \end{aligned}$$

This is not the case for a F-F input, as the photons arriving during the FT period, although mis-allocated into wrong CCD rows, will not always be lost. Let's assume the F-F image ("r" rows) is smaller than the number of CCD rows read out "R". Photons that arrive during the FT period are spread out over all 288 rows of the CCD. Those (mis-) allocated into the "R" rows are detected by the MIC system, while those in "288-R" rows are lost. Among the "R" events, "r" fall in the F-F image area and hence contribute to coincidence with events arriving in the imaging period following FT. The "R-r" events that fall outside of the F-F area do not suffer from such coincidence.

The effect of FT on coincidence loss should be very small if "r" is close to "R". Detected photons accumulated in a F-F image ("r" rows) are proportional to,

$$N_{\text{coince}} :: (\text{FT time}) \frac{r}{288} + (\text{Integration time})$$

Detected photons accumulated in the non-coincidence area (R-r) are proportional to,

$$N_{\text{non-coi}} :: (\text{FT time}) \frac{(R - r)}{288}$$

Detected photons are,

$$N_{\text{det}} = N_{\text{coince}} + N_{\text{non-coi}}$$

In the analysis carried out in this Report, all of the N_{det} were treated as being in the F-F area, which could cause inaccuracy. However, if adopting parameters for the DEP_#7 intensifier experiment,

$$\frac{N_{\text{non-coi}}}{N_{\text{coince}}} = \frac{0.2304\text{ms} \times (156\text{V}-129\text{V})/288\text{V}}{0.2304\text{ms} \times 129\text{V}/288\text{V} + 6.6222\text{ms}} = \frac{0.0216\text{ms}}{6.7254\text{ms}} = 0.0032$$

Therefore, the effect of FT could be ignored.

The number of events lost due to FT, as a ratio, can be described as follows,

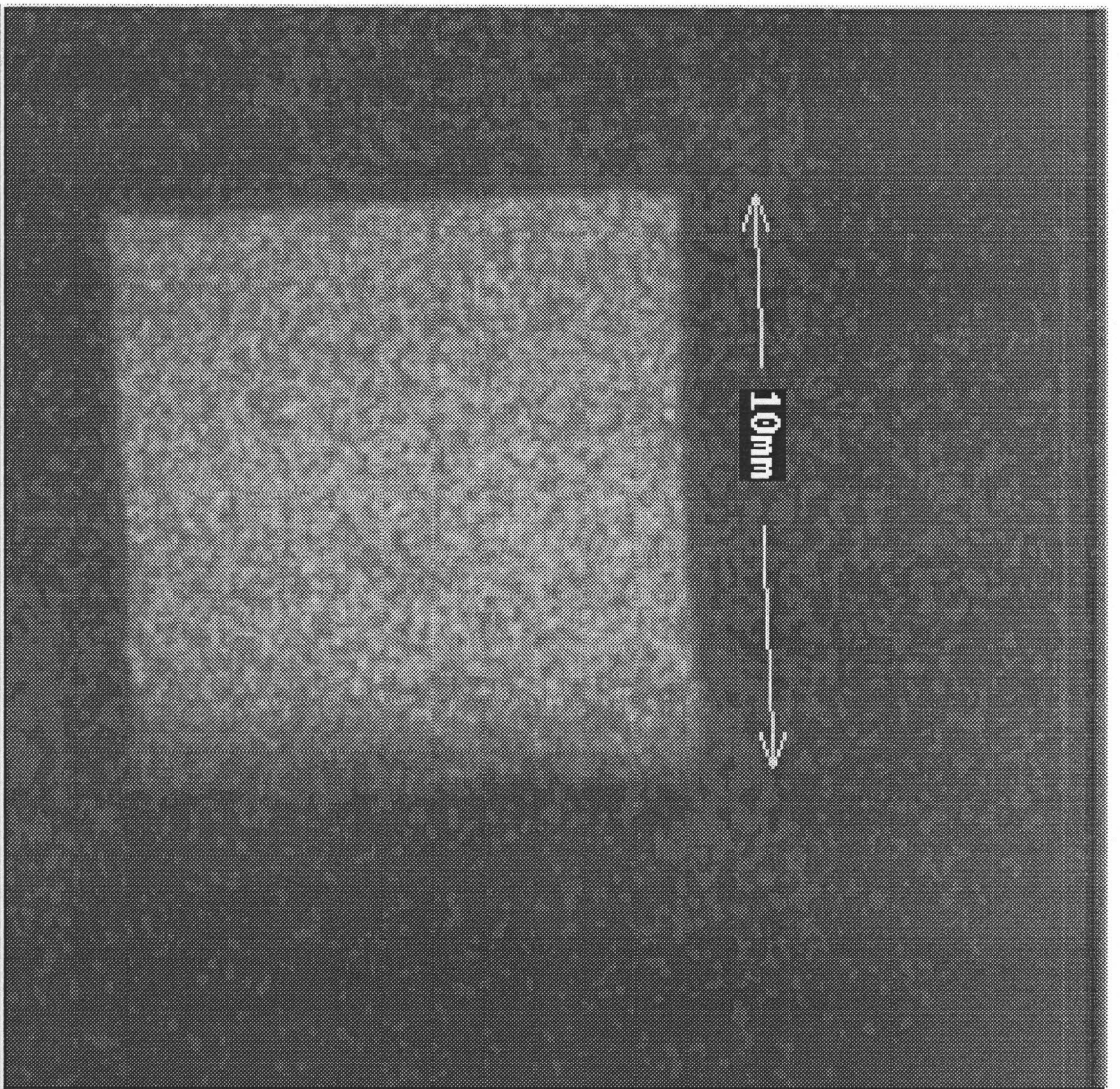
$$\frac{(\text{FT time})}{(\text{frame time})} \times \frac{(288 - R)}{288}$$

Where, $R > r$ is assumed.

In the case of DEP_#7 intensifier, $R=156\text{V}$, $r=129\text{V}$ (10mm), therefore event loss ratio is

$$0.2304\text{ms} \times (288-156) / (6.8526\text{ms} \times 288) = 0.01541$$

Note: The D.Q.E. value for the MIC photon counting detector must be corrected by a factor of $\times 1.015$, because the reference photo-diode captures photons without a dead time.



←————— 256 CCD pixels —————→

17H 29M 11S 17H 30M 35S 1998/10/12/
ANAZZ7 Mask for DQE DEP_#6 Ha1 40U SW=5um & 120um 5900A CCDst=1U

Fig. 1

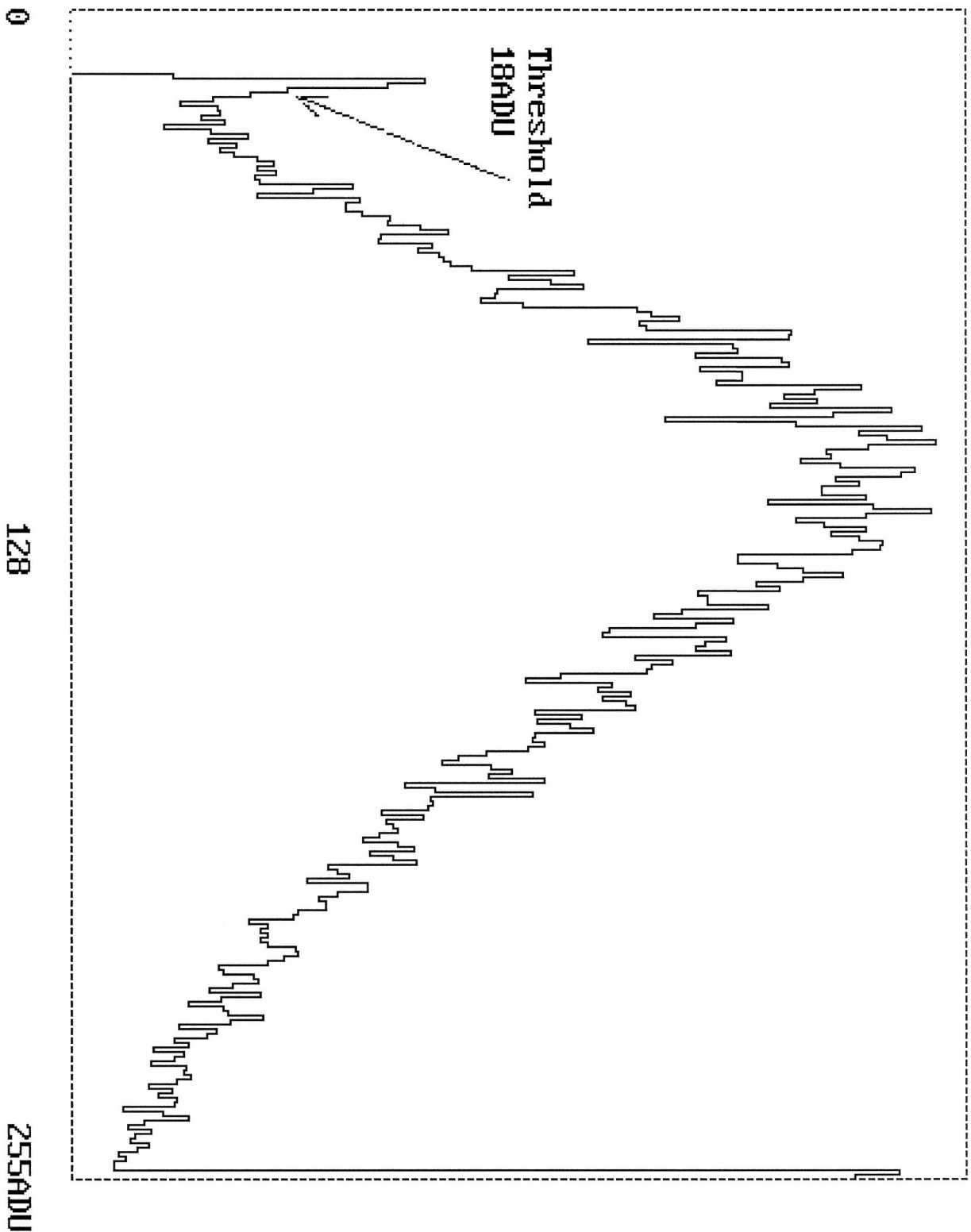


Fig 2b
Pulse Height Distribution of DEP_#7 intensifier 400-2420-5250 volts

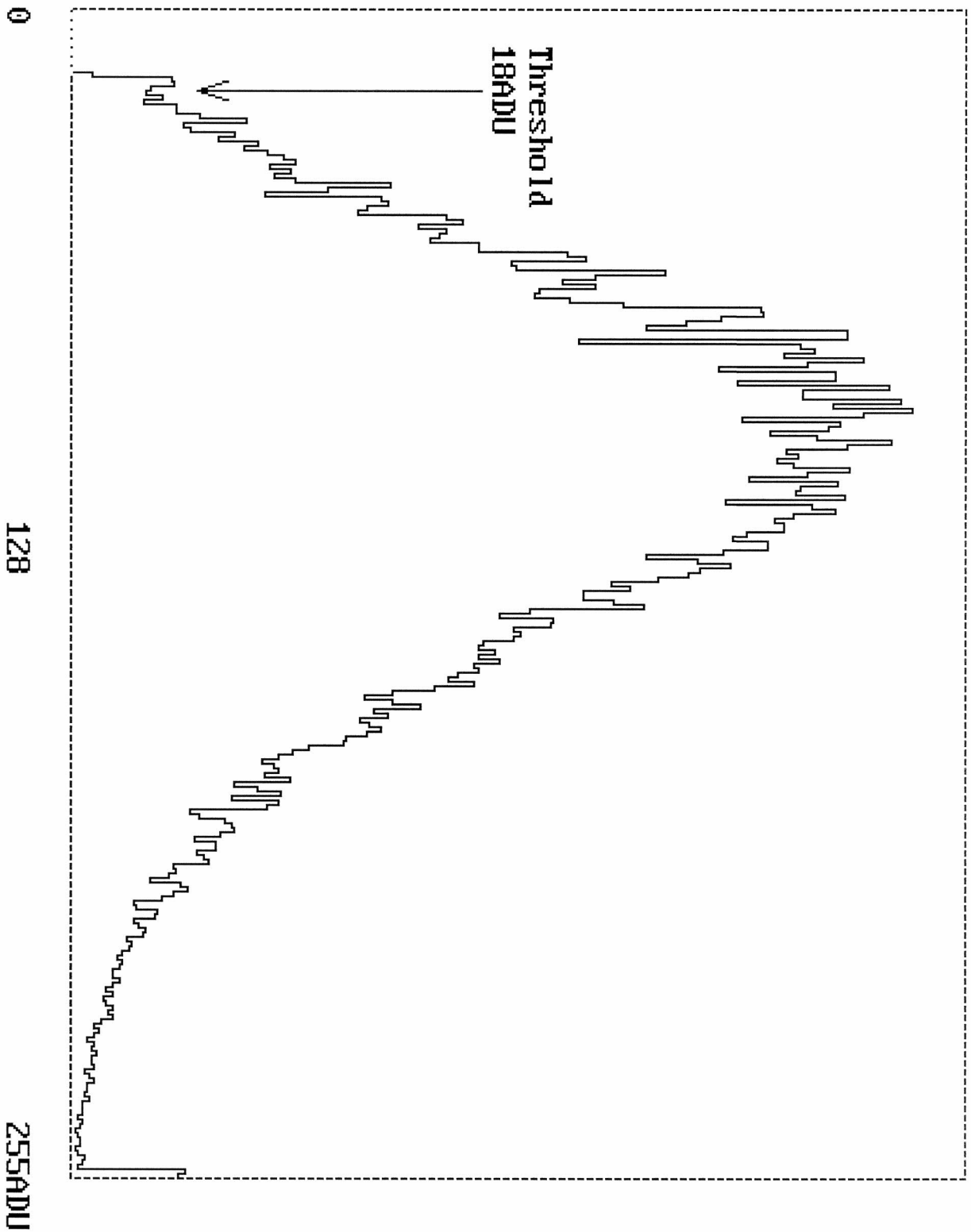


Fig 2a
Pulse Height Distribution of DEP_#6 intensifier 400-2400-5220 volts

